TU Delft

Delft University of Technology

Document Version
Final published version

Citation (APA)
Zhang, L., Li, G., Chen, H., Tang, J., Yang, G., Yu, M., Hu, Y., Xu, J., & Sun, J. (2024). Identification and Suppression of Multicomponent Noise in Audio Magnetotelluric Data Based on Convolutional Block Attention Module. *IEEE Transactions on Geoscience and Remote Sensing*, *62*, Article 5905515. https://doi.org/10.1109/TGRS.2024.3361942

Important note
To cite this publication, please use the final published version (if applicable).
Please check the document version above.

Copyright
In case the licence states “Dutch Copyright Act (Article 25fa)”, this publication was made available Green Open Access via the TU Delft Institutional Repository pursuant to Dutch Copyright Act (Article 25fa, the Taverne amendment). This provision does not affect copyright ownership.
Unless copyright is transferred by contract or statute, it remains with the copyright holder.

Sharing and reuse
Other than for strictly personal use, it is not permitted to download, forward or distribute the text or part of it, without the consent of the author(s) and/or copyright holder(s), unless the work is under an open content license such as Creative Commons.

Takedown policy
Please contact us and provide details if you believe this document breaches copyrights.
We will remove access to the work immediately and investigate your claim.

This work is downloaded from Delft University of Technology.

Green Open Access added to TU Delft Institutional Repository

'You share, we take care!' - Taverne project

https://www.openaccess.nl/en/you-share-we-take-care

Otherwise as indicated in the copyright section: the publisher is the copyright holder of this work and the author uses the Dutch legislation to make this work public.

Identification and Suppression of Multicomponent Noise in Audio Magnetotelluric Data Based on Convolutional Block Attention Module

Liang Zhang, *Member, IEEE*, Guang Li, Huang Chen, Jingtian Tang, Guanci Yang, Mingbiao Yu, *Member, IEEE*, Yong Hu, Jun Xu, and Jing Sun

***Abstract*— Audio magnetotelluric (AMT) is commonly used in mineral resource exploration. However, the weak energy of AMT signals makes them susceptible to being overwhelmed by noise, leading to erroneous geophysical interpretations. In recent years, deep learning has been applied to AMT denoising and has shown better denoising performance compared to traditional methods. However, current deep learning denoising methods overlook the characteristics of AMT signals, resulting in reduced denoising accuracy. To enhance the denoising performance of deep learning by better matching the features of AMT signals, we propose a convolutional block attention module (CBAM)-based method for AMT denoising. This method focuses on the features of AMT signals and improves the process from three aspects: 1) in the establishment of the sample set, we adopt a multicomponent form based on the correlation of noise to enable the neural network to explore the potential connections among the components of AMT during the training process, thus constructing a stronger network mapping relationship; 2) in the construction of the neural network, we have introduced the CBAM structure into the residual blocks of the ResNet to enhance the network's feature learning capability by focusing on the characteristics of noise; and 3) in the design of the denoising procedure, we adopt a process of identification before denoising to protect the noise-free data segments from being compromised during the denoising process. Finally, through synthetic, field data experiments, and comparative tests, we demonstrate that our proposed method achieves higher denoising accuracy than some traditional methods and conventional deep learning methods.**

***Index Terms*— Audio magnetotelluric (AMT), convolutional block attention module (CBAM), denoising, ResNet.**

Manuscript received 20 November 2023; revised 10 January 2024; accepted 26 January 2024. Date of publication 5 February 2024; date of current version 14 February 2024. This work was supported in part by the National Key Research and Development Program of China under Grant 2023YFF0718000; in part by Guizhou University Basic Research Project under Grant [2023]44; in part by the National Natural Science Foundation of China under Grant 41904076, Grant 42364006, and Grant 62163007; in part by Jiangxi Provincial Natural Science Foundation under Grant 20232BCJ23051, Grant 20232BAB203070, and Grant 20212BAB203004; in part by Guizhou Provincial Science and Technology Projects under Grant PTRC[2020]6007-2; and in part by China Postdoctoral Science Foundation under Grant 2021M703580. *(Corresponding authors: Guang Li; Huang Chen.)*

Liang Zhang, Guanci Yang, Mingbiao Yu, and Jun Xu are with the Key Laboratory of Advanced Manufacturing Technology, Ministry of Education, Guizhou University, Guiyang 550025, China (e-mail: liangzhang@gzu.edu.cn; gcyang@gzu.edu.cn; mbyu@gzu.edu.cn; 1815724800@qq.com).

Guang Li is with the Nanchang Key Laboratory of Intelligent Sensing Technology and Instruments for Geological Hazards and the Fundamental Science on Radioactive Geology and Exploration Technology Laboratory, East China University of Technology, Nanchang 330013, China (e-mail: li_guangg@163.com).

Huang Chen is with the School of Resources and Safety Engineering, Chongqing University, Chongqing 400044, China (e-mail: chenhuang@cqu.edu.cn).

Jingtian Tang is with the School of Geosciences and Info-Physics, Central South University, Changsha 410083, China (e-mail: jttang@mail.csu.edu.cn).

Yong Hu is with the School of Resources and Geosciences, China University of Mining and Technology, Xuzhou 221008, China, and also with the School of Geosciences, China University of Petroleum (East China), Qingdao 266580, China (e-mail: huyong@cumt.edu.cn).

Jing Sun is with the Intelligent Systems Department, Delft University of Technology, 2600 AA Delft, The Netherlands (e-mail: Jing.Sun@tudelft.nl).

Digital Object Identifier 10.1109/TGRS.2024.3361942

I. Introduction

AUDIO magnetotelluric (AMT) is a commonly used geophysical exploration method that offers several advantages. AMT utilizes natural sources and is not affected by near-field effects. The portability of AMT instruments makes them easy to transport. Additionally, AMT operates over a wide frequency range, enabling a broad exploration coverage. Being a tensor measurement, AMT captures data in both TE and TM modes, facilitating the identification of geological structures [1], [2]. Therefore, AMT plays a crucial role in mineral resource exploration. However, AMT signals are often contaminated by noise from sources such as signal towers, high-voltage lines, and various vehicles. Failure to remove such noise hampers the attainment of reliable geophysical interpretations [3].

Over the past few decades, numerous AMT denoising methods have been proposed. One effective approach is the remote reference method, which demonstrates good performance in AMT noise suppression. This method utilizes the magnetic field component of a remote reference point and the electric field component of the measurement point to compute the cross-power spectrum, rather than the auto-power spectrum [4]. However, a major drawback of this method is its reliance on a remote reference point. As cities rapidly develop, it becomes increasingly challenging to find suitable remote reference points. When an unreasonable remote reference point is selected, the effectiveness of this method diminishes [5]. Robust estimation techniques also play a crucial role in noise removal. Methods such as the M-regression estimator [6], bounded influence estimator [7], and repeated median estimator [8] are capable of suppressing noise influence and providing robust impedance estimation when the quality data section constitutes the majority. However, these methods have their limitations. For instance, the M-regression estimator is weak against magnetic noise influence, and all three mentioned methods are unable to effectively handle long-period noise that persists throughout the entire time series [9]. In addition

1558-0644 © 2024 IEEE. Personal use is permitted, but republication/redistribution requires IEEE permission.
See https://www.ieee.org/publications/rights/index.html for more information.

Authorized licensed use limited to: TU Delft Library. Downloaded on February 20,2024 at 08:28:18 UTC from IEEE Xplore. Restrictions apply.

to remote reference and robust estimation, inversion techniques have proven helpful in AMT denoising. Methods like Dplus and Rhoplus can rectify the noise influence on apparent resistivity. However, these methods require a majority of apparent resistivity points to be free from severe noise influence [10], [11].

Considering the limitations of remote reference, robust estimation, and inversion in AMT denoising, the time–frequency denoising method has gained popularity. This method proves effective in scenarios where remote reference points are not available, there is long-period noise in the time series, and the majority of apparent resistivity points are corrupted by noise. By filtering noise in the time series before impedance estimation, this method helps avoid distortion in impedance. Mathematical morphology filtering (MMF) is one of the time–frequency denoising methods that can be directly applied to the time series to suppress noise. However, MMF suffers from the loss of low-frequency information [12]. Empirical mode decomposition (EMD) is another approach that adaptively decomposes the AMT signal into several intrinsic mode functions (IMFs) and a residual component, preserving the low-frequency information while removing noise. However, EMD is prone to mode mixing, which leads to poor denoising performance [13]. To address the issue of mode mixing, researchers have developed various improvement methods, including improved complete ensemble EMD with adaptive noise (ICEEMDAN) [14] and variational mode decomposition (VMD) [15]. ICEEMDAN introduces white noise into the IMFs to tackle mode mixing, which improves denoising accuracy compared to EMD but introduces noise contamination to the IMFs [16]. On the other hand, VMD addresses mode mixing without adding noise, thus avoiding noise contamination in the IMFs. VMD approaches mode mixing from the perspective of Wiener filtering and requires the IMFs to be amplitude-modulated and frequency-modulated time series with limited bandwidth. The decomposition number in VMD can be set manually, and the envelope of the Hilbert transform of the signal can be useful in determining reasonable parameters to solve the mode mixing issue [17]. However, when the noise is severe and exists in all IMFs, VMD may not effectively handle it.

In addition to mathematical decomposition methods, sparse representation methods are also commonly used in AMT denoising. These methods leverage the fact that the effective AMT signal exhibits behavior similar to white noise. The noise-contaminated AMT signal is first projected onto a transform domain, where the noise and effective AMT signal can be separated based on their different distributions. Subsequently, further filtering is applied to achieve signal-noise separation [18]. The wavelet transform is widely employed in AMT signal denoising due to its excellent time–frequency analysis capabilities. Unlike the fixed time window in the short-time Fourier transform, the time window of the wavelet transform is adaptive through the translation and expansion of the wavelet basis, enabling accurate AMT denoising. In general, the coefficients corresponding to noise are larger than those of the effective AMT signal in the wavelet domain. Thus, appropriate thresholds can be set to extract the noise [19]. However, a limitation of the wavelet transform is that the choice of wavelet basis is fixed and cannot be changed during denoising, which can impact noise suppression. Dictionary learning methods provide an adaptive representation of noise during denoising by iteratively updating the coefficients and the learning basis. This leads to accurate noise removal. Examples of such methods include K-singular value decomposition (KSVD) [20], shift-invariant sparse coding (SISC) [21], and data-driven tight frame (DDTF) [22]. DDTF is an improved dictionary learning method for KSVD that enhances the running speed by incorporating a tight frame. However, dictionary learning may introduce new noise due to the lack of prior signal construction information [23].

The development of deep learning techniques in recent years has had a profound and lasting impact on noise suppression. Compared to mathematical decomposition methods such as MMF, EMD, and VMD, deep learning demonstrates superior capability in suppressing severe noise by training models to establish the mapping relationship between input and labels. Unlike sparse representation, deep learning does not rely on the assumption of signal sparsity, resulting in enhanced denoising performance [24]. Deep learning has found extensive applications in electromagnetic noise reduction, employing techniques such as long short-term memory (LSTM) networks [25], convolutional neural networks (CNNs) [26], ResNet [27], and U-Net [28]. However, conventional neural networks often overlook the specific characteristics of AMT signals, leading to a decrease in denoising performance. There are two key characteristics of noise that must be considered in AMT denoising. First, noise exhibits temporal correlation in its distribution, affecting both the AMT electric and magnetic channels simultaneously. Neglecting this characteristic and denoising each channel separately may result in the omission of noisy data segments. Second, short-period noise is localized and introduces only local interference to the AMT time series. Denoising the entire time series may potentially damage noise-free segments. Therefore, a careful approach is required to mitigate this issue. Furthermore, improving the neural network's ability to learn noise features poses another challenge in AMT denoising. It is crucial to design neural network architectures that effectively capture and discriminate noise characteristics in AMT signals to achieve better denoising performance.

In summary, the current methods for AMT denoising have certain limitations. Traditional approaches like mathematical decomposition and sparse representation suffer from low accuracy, while methods such as remote reference, robust estimation, and inversion lack universality. Although deep learning methods have shown promise in addressing these limitations, they also have their own drawbacks. For instance, they often overlook the distinctive features of AMT signals and their feature learning capabilities still need improvement. These challenges highlight the potential for further advancements in the field of AMT denoising.

To enhance the performance of deep learning in AMT denoising, we propose a method called convolutional block attention module (CBAM) for identifying and suppressing multicomponent noise in AMT signals. This method utilizes a time window to extract time series from multiple components of AMT electric and magnetic channels, constructing a

Authorized licensed use limited to: TU Delft Library. Downloaded on February 20,2024 at 08:28:18 UTC from IEEE Xplore. Restrictions apply.

multicomponent sample set that allows the neural network to capture the relevant features of the noise during the training process. As a result, a more robust mapping relationship is established. To address the issue of localized concentration of short-period noise, the method adopts a two-step process of noise identification followed by denoising, aiming to preserve the segments without noise as much as possible and only denoise the segments with noise. Additionally, CBAM is incorporated into the residual network to enhance the network's ability to learn signal features. Finally, through experiments on both synthetic and field data, this study verifies that the proposed method not only effectively removes noise in AMT data, but also outperforms some traditional AMT denoising methods in terms of denoising performance.

II. Methodology

In the context of deep-learning-based AMT denoising, the neural network updates its parameters $\theta\{w, b\}$ (including weights w and biases b) through training to learn a mapping relationship $\varphi(\cdot)$ from samples F to labels $\hat{F}$. F consist of multiple noisy AMT signals f, while $\hat{F}$ consist of corresponding clean AMT signals $\hat{f}$. Let f_i, $\hat{f}_i$, and $\tilde{f}_i = \varphi(f_i; \theta)$ denote the ith sample, label, and the corresponding neural network output, respectively. N denotes the total number of samples. The network training can be seen as optimizing $\theta\{w, b\}$ and the objective function $L(\theta)$ in the following, subject to an L2-norm constraint:

$$L(\theta) = \frac{1}{2N}\sum_{i=1}^{N}\left\|\tilde{f}_i - \hat{f}_i\right\|_2^2 = \frac{1}{2N}\sum_{i=1}^{N}\left\|\varphi(f_i;\theta) - \hat{f}_i\right\|_2^2. \quad (1)$$

N represents the number of samples. In this study, we employ the ADAM optimizer [29] to optimize (1). Once the network training is completed, the noisy AMT signals f can be inputted into the network, and the denoised AMT signals $\bar{f}$ can be obtained based on the learned mapping relationship.

Fig. 1 illustrates the complete denoising process of our method. From Fig. 1, it can be observed that our method consists of three main components: the establishment of the sample set, the construction of the neural network, and the design of the denoising procedure.

The steps for acquiring the sample set are as follows: select an equal number of synthetic and field AMT data; use a time window to extract time series from multiple components of AMT channels (electric and magnetic) within the same time interval; repeat the previous step to obtain a large number of multicomponent samples, where each sample contains time series from the same time interval of the channels; mark the samples differently based on the specific purpose (identification or denoising); and obtain the identification sample set and the denoising sample set.

The steps for designing the neural network are as follows: construct the CBAM structure; add the CBAM structure to the ResNet, completing the construction of the neural network architecture; initialize the parameters of the constructed neural network; load the sample set and train the network; fine-tune the parameters until the loss function converges satisfactorily; save the trained network when the loss converges; and depending on the input sample set (identification or denoising), the saved neural network will differ (identification network or denoising network).

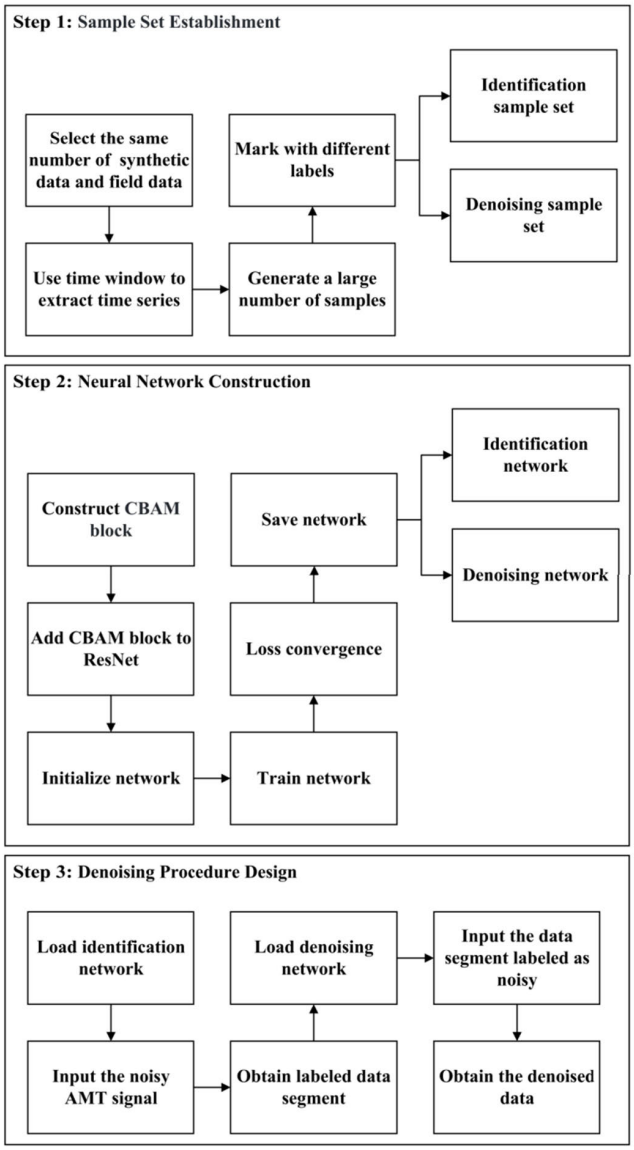

Fig. 1. Implementation process of the method in this article.

The steps for data denoising are as follows: load the saved identification network; input the AMT signal that needs to be denoised; obtain the labeled data segment; load the saved denoising network; input the data segment labeled as noisy; and obtain the denoised AMT data.

In Sections II-A–II-C, this article will provide a detailed exposition of the establishment of the sample set, the construction of the neural network, and the design of the denoising procedure, as described above.

A. Sample Set Establishment

During the process of selecting data to construct the sample set, two challenges commonly arise: noise interference and a lack of realism [30]. If the sample set consists solely of field data, it becomes difficult to avoid noise regardless of

Authorized licensed use limited to: TU Delft Library. Downloaded on February 20,2024 at 08:28:18 UTC from IEEE Xplore. Restrictions apply.

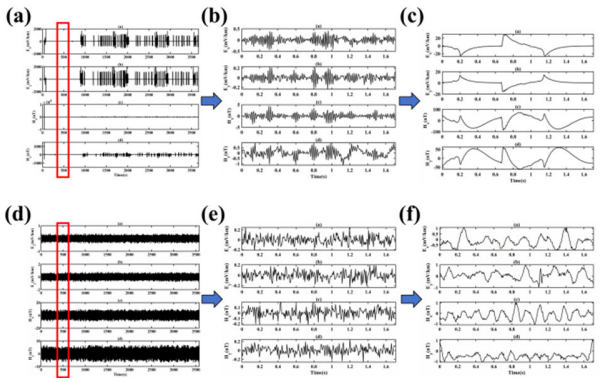

Fig. 2. Sample selection process. (a) and (d) Field and synthetic AMT time series, respectively; (b) and (e) Selected field and synthetic data segments, respectively; (c) and (f) Field and synthetic data segments after noise addition, respectively.

how the samples and labels are chosen. This compromises the mapping relationship established by the neural network, resulting in decreased denoising effectiveness. Conversely, if the sample set is exclusively composed of synthetic data, although it eliminates noise interference in the samples and labels, the mapping relationship constructed through network training struggles to accurately match the mapping patterns of field data, leading to subpar denoising performance. To strike a balance between these two factors, we adopt an approach that involves constructing the sample set using an equal number of synthetic and field data. The synthetic data serve the purpose of suppressing noise interference in the field data, while the field data compensate for the limitations of the synthetic data in representing real-world scenarios. In this study, the synthetic data, which incorporates geological layers, are generated through forward modeling and are obtained from the open-source code available at https://github.com/EMWPJ/SyntheticMTTimeSeries [31]. The field data are collected in the Tongling area of Anhui, China, using the V-5 instrument manufactured by Phoenix Geophysics, Toronto, ON, Canada. Consequently, the accompanying software, SSMT2000, is employed for calculating apparent resistivity and phase in this study.

Our strategy for constructing the sample set involves scanning the synthetic and field AMT time series using a time window and extracting the scanned data segments. Subsequently, noise is added to the data segments to form sample-label pairs. Fig. 2 illustrates the process of selecting samples using a time window. For the field data shown in Fig. 2(a), we use a time window [indicated by the red box in Fig. 2(a)] to select data segments from the four components (electric and magnetic channels) within the same time interval, ensuring their correlation. The selected data segments, with minimal noise interference, are depicted in Fig. 2(b). Subsequently, we manually introduce noise to these data segments, resulting in the noisy segments shown in Fig. 2(c). It is worth noting that when selecting field data, priority is given to the time series of the target denoising point. The manually added noise corresponds to the noise present in that specific measurement point (obtained through other denoising methods, such as the DDTF used in this study). Moreover, the noise is also generated from data segments

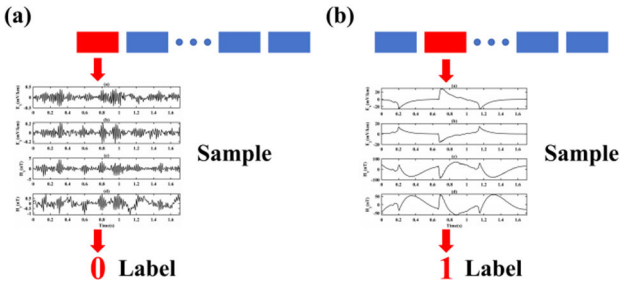

Fig. 3. Samples and labels in the identification sample set. (a) and (b) Noise-free and noisy data segments, respectively.

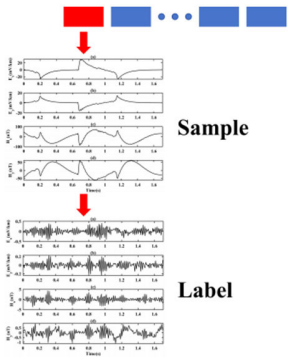

Fig. 4. Samples and labels in the denoising sample set.

selected using the time window from the electric and magnetic channels, ensuring their correlation. If the target denoising point is severely affected by noise, making it difficult to select data segments with minimal noise, adjacent measurement points with less noise interference are chosen to ensure that the mapping relationship obtained after network training can better match the actual conditions of the target point. For the synthetic data in Fig. 2(d), the selection process is similar to that of real data. Although it eliminates noise interference, there are important considerations when selecting the data: the added noise should resemble the form and amplitude of the noise present in the field data. For example, if the noise in the target denoising point of the field data mainly consists of discharge triangle waves and harmonics without square waves, the added noise in the synthetic data should primarily consist of discharge triangle waves and harmonics, without square waves. Additionally, the maximum amplitude of the added noise should not exceed the maximum amplitude of the noise in the field data by a large margin. Furthermore, it is essential to ensure the correlation of the added noise.

We follow the approach depicted in Fig. 2 to select samples, and the construction of the sample sets differs based on the specific objectives of identification and denoising. Figs. 3 and 4 illustrate the identification sample set and the denoising sample set we created, respectively. In Figs. 3 and 4, rectangles represent samples, the red rectangle represents the currently displayed sample, and ellipses indicate samples not shown. From Fig. 3, we can observe that the identification sample set consists of both noise-free multicomponent data segments and noisy multicomponent data segments. These two types of data segments each account for 50% of the sample set. The noise-free data segments are labeled as 0, while the noisy data segments are labeled as 1. In Fig. 4,

Authorized licensed use limited to: TU Delft Library. Downloaded on February 20,2024 at 08:28:18 UTC from IEEE Xplore. Restrictions apply.

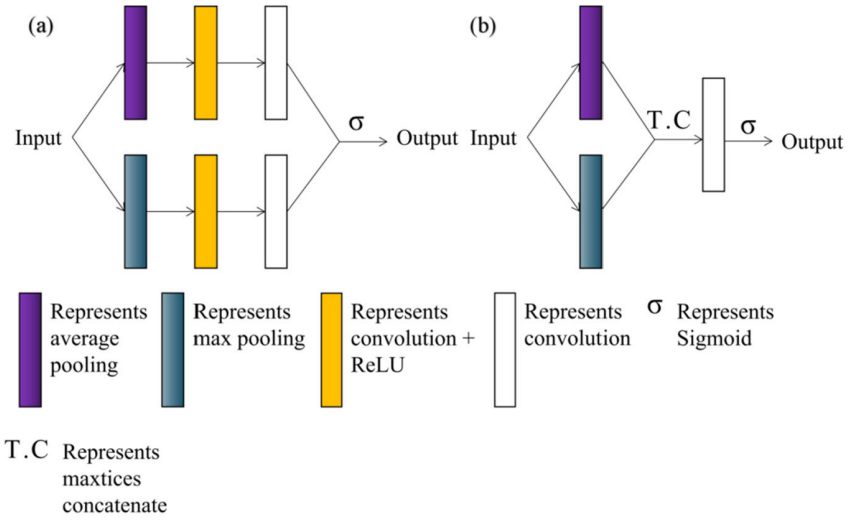

Fig. 5. CBAM. (a) Channel attention. (b) Spatial attention.

we can see that the denoising sample set solely comprises noisy multicomponent data segments, with the labels being the corresponding noise-free multicomponent data segments. In the identification and denoising sample sets used in this study, both training and validation sets are included. The training set contains 100 000 samples, and the validation set contains 10 000 samples. The synthetic data and field data each contribute 50% of the total sample count.

After constructing the sample set, we performed a preprocessing step of maximum-minimum normalization exclusively on the sample set before network training. This involved proportionally scaling the values in the sample set to the interval of $[-1, 1]$. The purpose of this normalization was to prevent gradient vanishing and exploding during network training, thereby enhancing network stability and expediting the training process.

B. Neural Network Construction

ResNet has demonstrated strong feature learning capabilities and has been widely applied in the field of geophysics due to its simplicity in construction, ease of parameter tuning, and training [32], [33], [34]. The residual block structure in ResNet can be seen as a shortcut from shallow layers to deep layers, ensuring that feature information is not lost during network training and avoiding the problem of network degradation that can occur with increasing layer depth [35]. To further enhance the feature extraction capability of ResNet, this study introduces the CBAM structure into ResNet. CBAM possesses a unique information weighting capability, enabling the network to perform weighted processing on both channel and spatial information. This allows the network to focus on important feature information while disregarding the influence of irrelevant information, thus enhancing the network's feature-learning capability [36]. CBAM consists of two structures: channel attention and temporal attention, as shown in Fig. 5.

In the channel attention mechanism depicted in Fig. 5(a), the input information is initially fed into average pooling w_{avg} and max pooling layers $w_{\max}$, respectively. Subsequently, the results from these two pooling operations are separately processed through convolutional layers, ReLU activation functions, and additional convolutional layers w_{cr}. The outputs of these operations are then summed together. Finally, the resulting sum is passed through a Sigmoid activation function σ to produce the final output. Consequently, the steps involved in the channel attention mechanism can be described as follows:

$$\text{Output} = \sigma\left(w_{\text{cr}}\left(w_{\text{avg}}(\text{Input})\right) + w_{\text{cr}}(w_{\max}(\text{Input}))\right). \quad (2)$$

In the spatial attention mechanism illustrated in Fig. 5(b), the input information is initially fed into w_{avg} and $w_{\max}$, respectively. Subsequently, the results from these two pooling operations are concatenated together $T \cdot C(\cdot)$ to form a unified matrix. This matrix is then processed through convolutional layers w_c and passed through σ. Finally, the resulting output is obtained. Therefore, the steps involved in the spatial attention mechanism can be described as follows:

$$\text{Output} = \sigma\left(w_c\left(T \cdot C\left(w_{\text{avg}}(\text{Input}), w_{\max}(\text{Input})\right)\right)\right) \quad (3)$$

by utilizing (2) and (3), neural networks not only have the capability to adaptively learn the weights of input information in both the channel and spatial dimensions, thereby emphasizing important features within these dimensions, but they can also enhance their feature learning capabilities by combining the two attention mechanisms to learn the correlation between important features in both channel and spatial domains [37]. Furthermore, it has been demonstrated that applying channel attention first followed by spatial attention yields superior results compared to the reverse order [38].

We incorporate CBAM into the residual block structure of ResNet, resulting in the architecture shown in Fig. 6. Fig. 6(a) represents the CBAM residual block structure when the input and output dimensions are consistent. However, when the input and output dimensions are inconsistent, a convolutional layer is employed in the shortcut branch of the CBAM residual block [Fig. 6(a)] to adjust the dimensions, leading to the CBAM residual block shown in Fig. 6(b). Finally, we replace the residual blocks in ResNet with the two types of CBAM residual blocks depicted in Fig. 6, resulting in the design of our neural network architecture, as shown in Fig. 7. The parentheses and ellipsis in Fig. 7 indicate the alternation and

Authorized licensed use limited to: TU Delft Library. Downloaded on February 20,2024 at 08:28:18 UTC from IEEE Xplore. Restrictions apply.

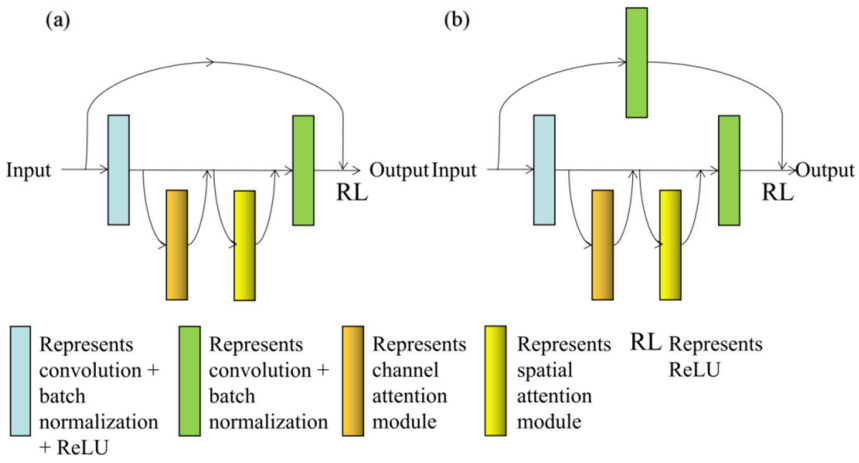

Fig. 6. CBAM residual block structure. (a) and (b) CBAM residual block when the input and output sizes are consistent and inconsistent, respectively.

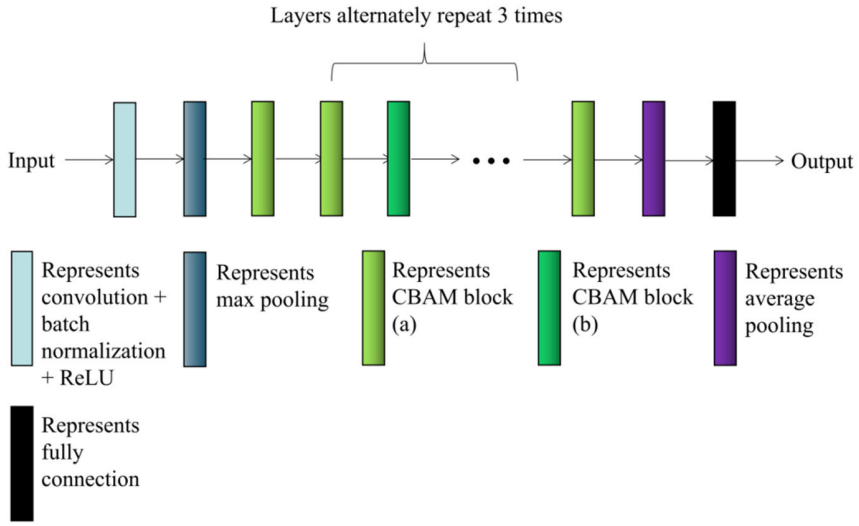

Fig. 7. Neural network structure used in this article.

repetition of the CBAM residual blocks (a) from Fig. 6(a) and the CBAM residual blocks (b) from Fig. 6(b), repeated three times. We created two types of sample sets: an identification sample set and a denoising sample set. Therefore, the constructed network consists of two types: an identification network and a denoising network. These two networks share the same main structure, differing only in the loss function and the output interface size. For the identification network, we employ cross-entropy loss, and the output interface size depends on the dimensions of the labels (0 and 1). On the other hand, the denoising network utilizes the mean square error loss and the output interface size depends on the dimensions of the noise-free data. Once the identification network and denoising network are constructed, we load the identification sample set and the denoising sample set, respectively, for network training. After the loss converges, we save the trained neural networks for both types.

In order to facilitate the reproducibility of the experimental results presented in this article, we have made the code publicly available. The parameters of the neural network employed in this study, such as the sizes of the convolutional kernels and the stride values, can be accessed for reference at: https://github.com/zl175050483/CBAM_AMT_Denoising. The main architecture of the neural network in this article involves the addition of the CBAM structure on top of ResNet. To maintain stability between the two network structures, we have only modified the 18 layers ResNet [32] and CBAM [39] from a 2-D interface to a 1-D interface, without altering other main structural components. Consequently, the 3×3 convolutional kernel (used in ResNet) and the 7×7 convolutional kernel (used in spatial attention mechanism) have been transformed into 1×3 and 1×7, respectively. Different kernel sizes possess distinct receptive fields and exhibit varying levels of feature focus. Typically, smaller convolutional kernels pay more attention to detail, while larger kernels offer a better global perspective. The experimental data in this study primarily suffer from short-period noise interference. Hence, adopting smaller kernel sizes in the main framework of the network (i.e., ResNet) enables a better fit to the noise characteristics, while utilizing larger convolutional kernels in spatial attention compensates for the lack of global perspective [40].

Authorized licensed use limited to: TU Delft Library. Downloaded on February 20,2024 at 08:28:18 UTC from IEEE Xplore. Restrictions apply.

C. Denoising Procedure Design

After saving the trained neural network, we can utilize it to remove noise from the AMT time series. First, the stored identification network is loaded. Then, the noisy AMT time series is processed in segments according to the size of the sample set, as illustrated in Fig. 2(d) and (e). A time window is employed to scan the AMT time series, and the scanned data segments are extracted. The size of the time window matches that of the sample set during its creation, and the window moves forward by a certain stride (half the length of the time window in this study) after each extraction. This process continues until all data points on the AMT time series have been scanned and extracted, resulting in the obtained AMT data segments being ready for identification.

By inputting the AMT data segments to be recognized into the identification network, we obtain labeled AMT data segments. Segments labeled as 0 indicate noise-free data, while segments labeled as 1 represent data contaminated with noise. The positional indices of these segments labeled as 1 on the AMT time series are recorded. Subsequently, the denoising network is loaded, and only the segments labeled as 1 are fed into the denoising network, resulting in the generation of denoised data segments.

Finally, based on the recorded positional indices, the data segments on the AMT time series are replaced with their corresponding denoised segments. In cases where multiple segments overlap, the data points are averaged. After that, we can obtain the denoised AMT time series. This process allows for the removal of noise from the AMT data while prioritizing the preservation of noise-free segments, resulting in a highly accurate denoising of the AMT. The denoised AMT time series achieves a significant reduction in noise while minimizing any distortion to the original data.

III. Synthetic Data Experiments

To validate the effectiveness of the proposed method, we conducted synthetic data experiments. In these experiments, the signal-to-noise ratio (SNR) was utilized as a quantitative measure to assess the denoising performance. The SNR is employed to compare the noise-free AMT signal $\hat{f}$ with the denoised AMT signal $\tilde{f}$, and it can be expressed as follows:

$$\mathrm{SNR} = 10\log_{10}\left(\frac{\|\hat{f}\|_2^2}{\|\hat{f}-\tilde{f}\|_2^2}\right). \tag{4}$$

The synthetic data utilized in this study are presented in Fig. 8, featuring a sampling rate of 150. Fig. 8 displays the noise-free AMT time series on the same time interval for both the electric and magnetic channels E_x, E_y, H_x, H_y, along with their respective outcomes subsequent to the introduction of noise. Notably, the noise was introduced within the time intervals of 14–33 and 46–60 s. The SNR of the AMT signals, subsequent to the addition of noise, is −20.00 dB.

A. Noise Identification

According to the denoising steps outlined in this study, the first step is to identify the noise. We set the time window

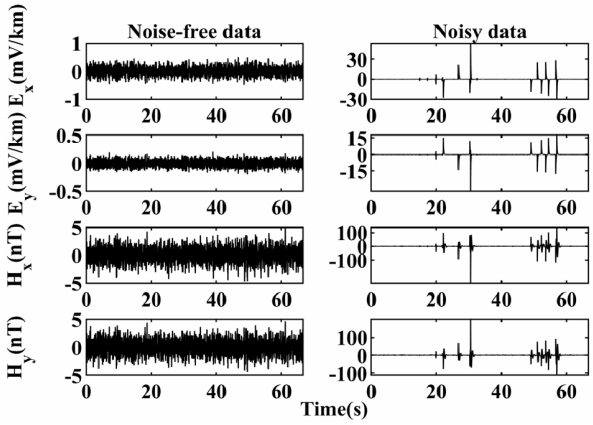

Fig. 8. Synthetic data with and without noise.

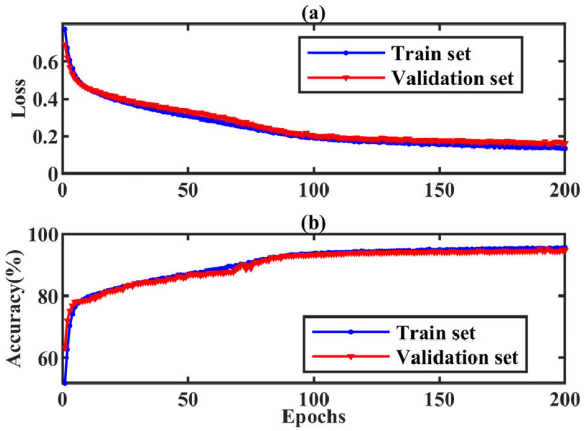

Fig. 9. (a) Loss and (b) accuracy of the identification network.

TABLE I
Impact of Different Length Time Windows on Identification Network

Length	Loss	Accuracy	Time (s)
128	0.2277	92.9%	5226
256	0.1426	95.3%	8195
512	0.1554	95.0%	13932
1024	0.1385	95.5%	29397

length to 256 to create the identification sample set. This sample set is then loaded into the identification network for training. The changes in loss and accuracy during training are shown in Fig. 9. From Fig. 9, it can be observed that as the epochs progress, the loss decreases and the accuracy increases for both the training and validation sets. When the epoch reaches 180, the loss and accuracy reach a plateau, indicating that the network has been trained sufficiently. Table I presents the changes in loss and accuracy when using different time window lengths to create the identification sample set. It can be observed from Table I that when the time window length is set to 256, 512, or 1024, there is little difference in loss and accuracy among them, and all of them outperform the results obtained with a time window length of 128. In general, longer samples tend to contain more features, which can be

Authorized licensed use limited to: TU Delft Library. Downloaded on February 20,2024 at 08:28:18 UTC from IEEE Xplore. Restrictions apply.

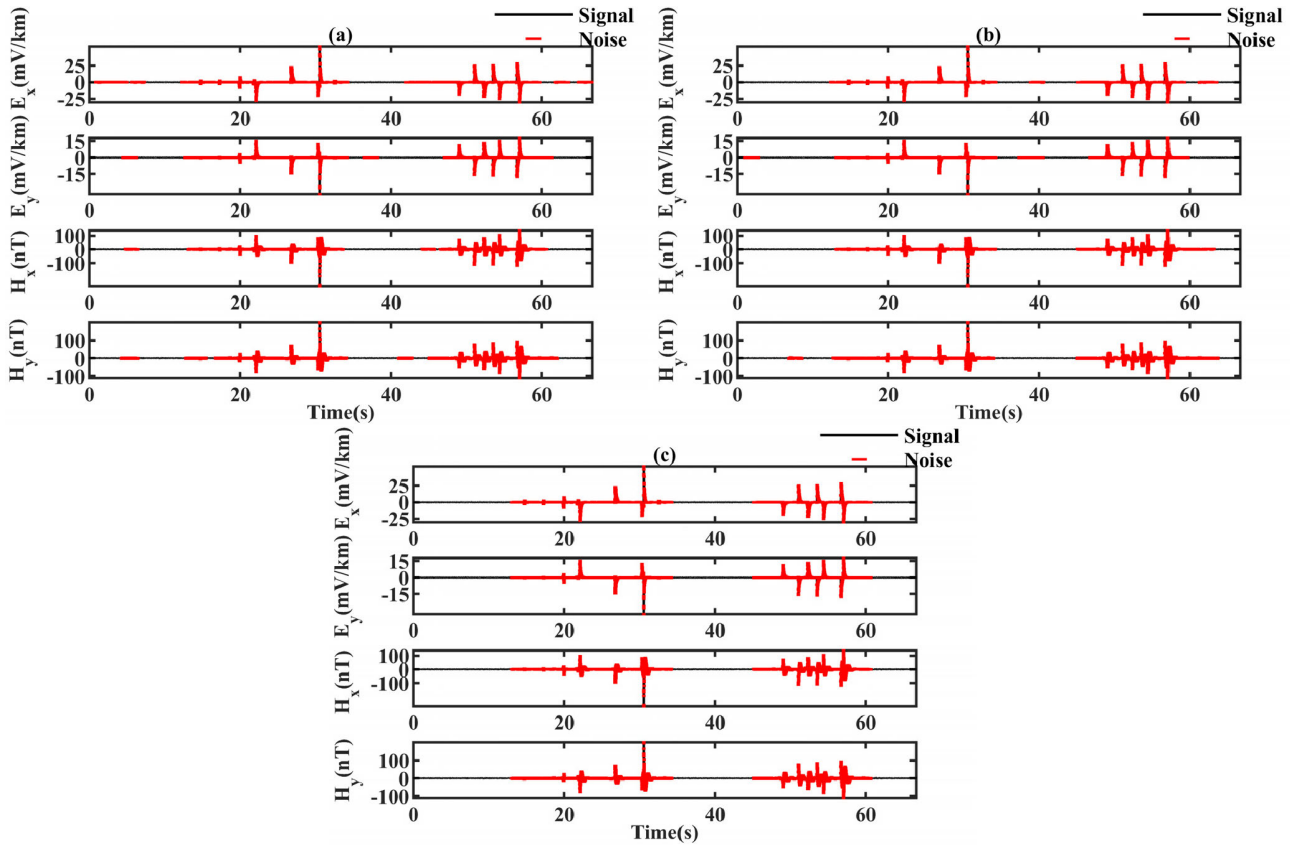

Fig. 10. Noise identification. (a) ResNet. (b) CBAM. (c) Proposed method.

advantageous for the network to learn better mapping relationships. However, in the context of this study, the experimental data are primarily affected by short-period noise. Therefore, a sample length of 256 is sufficient for the network to learn an adequate representation of the noise characteristics, yielding comparable results to samples of lengths 512 and 1024. Consequently, in order to achieve high recognition accuracy while minimizing time consumption, we selected samples of length 256 when constructing a dataset of 100 000 samples for identification.

Once the identification network has been trained, the noisy AMT time series can be inputted into the network for noise identification. To demonstrate the performance improvement achieved by adding the CBAM structure and using a multicomponent sample set, the noise identification results of the proposed method are compared with ResNet and CBAM. ResNet and CBAM use single-component sample sets, while the proposed method builds upon CBAM by employing a multicomponent sample set. The noise identification results of ResNet, CBAM, and the proposed method for the noisy synthetic AMT data in Fig. 8 are shown in Fig. 10(a)–(c), respectively. The accuracy of noise identification for ResNet, CBAM, and the proposed method is 91.4%, 93.6%, and 95.3%, respectively. The segments identified as containing noise by the networks are marked with red line segments in Fig. 10. From Fig. 10, it is evident that both ResNet and CBAM exhibit noticeable misclassifications in the noisy segments. Among them, CBAM demonstrates a lesser degree of misclassification compared to ResNet. Conversely, the proposed method achieves higher accuracy than both ResNet and

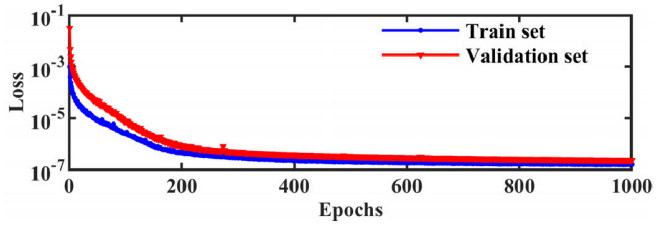

Fig. 11. Loss of the denoising network.

CBAM, effectively leveraging the correlation of the noise for noise identification. Consequently, in Fig. 10(c), no significant misclassifications in the data segments are observed. It is noteworthy that severely noisy data segments are predominantly identified by all three methods, and the misclassifications tend to occur in the noise-free segments. As a result, their impact on the final denoising outcome is not as pronounced. However, these misclassifications can introduce noise-free segments into the denoising network, thereby attenuating the denoising precision for these misclassified segments.

After noise identification, we can obtain the segments containing noise and record their positional indices in the AMT time series. We can then proceed to the noise suppression stage.

B. Noise Suppression

During the process of noise suppression, we exclusively focus on removing noise from the segments containing noise, ensuring that segments without noise are not inputted into the denoising network to preserve their integrity. Fig. 11 illustrates

Authorized licensed use limited to: TU Delft Library. Downloaded on February 20,2024 at 08:28:18 UTC from IEEE Xplore. Restrictions apply.

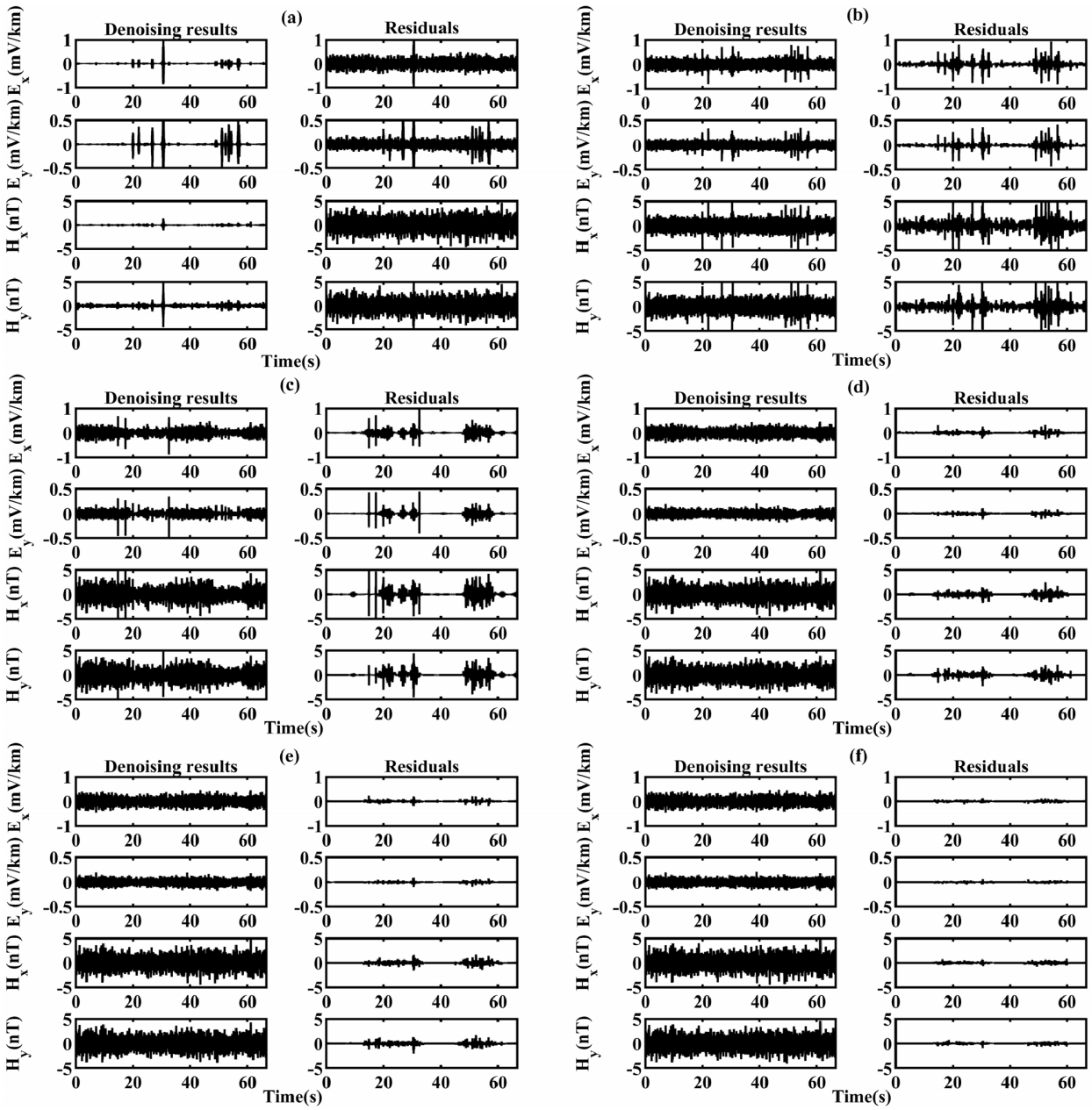

Fig. 12. Noise suppression. (a) VMD. (b) Wavelet transform. (c) DDTF. (d) ResNet. (e) CBAM. (f) Proposed method.

the variation of loss during the creation of the denoising sample set using a time window of length 256. It can be observed that as the number of epochs increases, the loss for both the training and validation sets gradually decreases. Beyond 900 epochs, the loss for both sets levels off, indicating the completion of network training. Table II presents the variation of loss obtained during training when using different lengths of time windows to create the denoising sample set. From Table II, it is evident that when the time window length is set to 256, 512, or 1024, the losses are similar and all lower than the loss obtained with a time window length of 128. Similar to constructing an identification sample set, this study selects a time window length of 256 to balance the training time and denoising ability when creating the denoising sample set.

TABLE II
IMPACT OF DIFFERENT LENGTH TIME WINDOWS ON DENOISING NETWORK

Length	Loss	Time (s)
128	2.7593×10^{-7}	33039
256	2.3805×10^{-7}	49164
512	2.3563×10^{-7}	86411
1024	2.4064×10^{-7}	178190

To facilitate the reproducibility of the experiments described in this article, we provide the specifications of the computer setup used in the experiments: CPU Intel i9-13900K, operating

Authorized licensed use limited to: TU Delft Library. Downloaded on February 20,2024 at 08:28:18 UTC from IEEE Xplore. Restrictions apply.

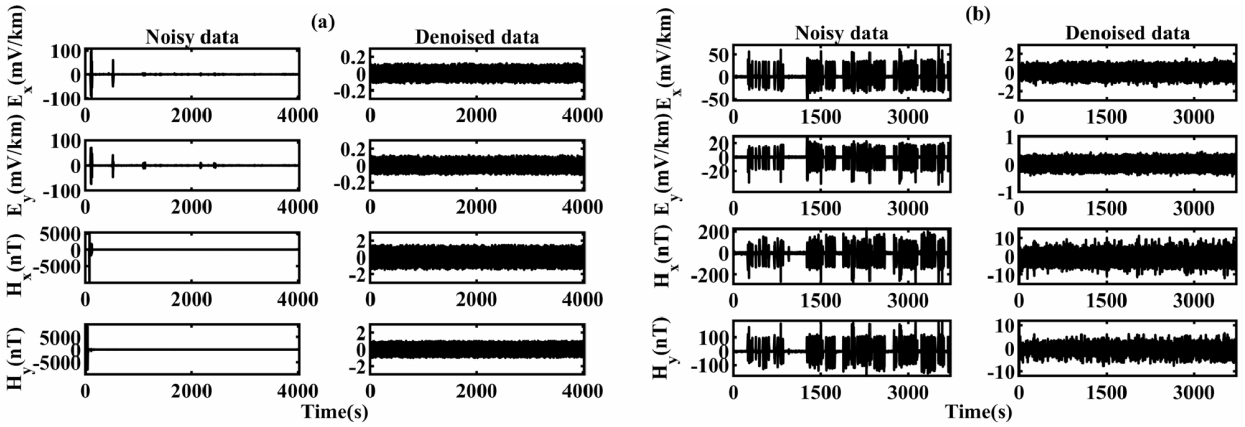

Fig. 13. Changes in time series before and after denoising for field data. (a) A121562A. (b) A121534A.

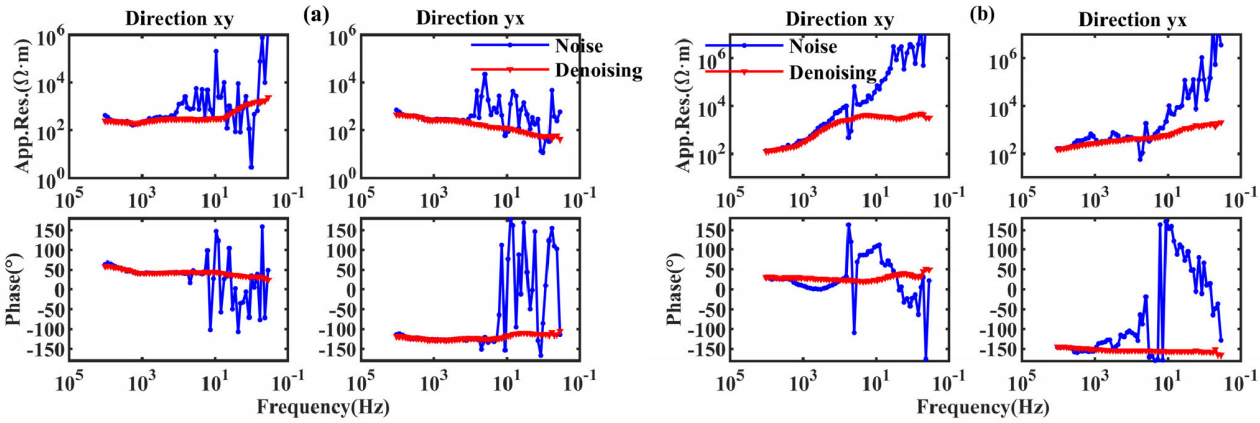

Fig. 14. Changes in apparent resistivity and phase before and after denoising for field data. (a) A121562A. (b) A121534A.

at a frequency of 5.50 GHz with 24 cores and GPU Nvidia GeForce GTX 4090 with 24 GB of memory.

After the completion of training the denoising network, the noisy data segments are fed into the network to obtain the denoised data segments. These denoised segments are then restored to the original noisy AMT time series based on the recorded position indices, thereby achieving high-precision AMT denoising. In the context of noise suppression, our approach is not only compared with the ResNet and CBAM models used for noise identification, but also with VMD, wavelet transform, and DDTF methods. Fig. 12(a)–(f) illustrates the denoising results and residuals (i.e., the differences between the denoised results and the noise-free data) for VMD, wavelet transform, DDTF, ResNet, CBAM, and our proposed method, with corresponding SNR values of 0.1028, 3.3953, 6.2739, 12.5593, 14.3841, and 20.3311 dB, respectively. From Fig. 12, it is evident that both VMD and wavelet transform yield poor denoising results. These methods exhibit significant degradation in the AMT signal while removing the noise. Particularly, VMD demonstrates severe degradation in the AMT signal, which may be attributed to its limited capability in handling pseudo-discharge triangular wave noise. It performs poorly when dealing with singular points in the noise. Although DDTF performs better than VMD and wavelet transform, it struggles to handle abrupt noise variations, resulting in substantial damage to the AMT signal in those regions. ResNet and CBAM demonstrate superior denoising results compared to DDTF, effectively handling noise variations. However, they also introduce some signal degradation at misidentified positions. Notably, CBAM inflicts less damage to the AMT signal than ResNet. Our proposed method outperforms the other denoising approaches, effectively mitigating noise influences, accurately identifying noise-free segments, and causing minimal degradation to the AMT signal compared to the other methods.

IV. Field Data Experiments

In these field data experiments, we selected two measurement points, A121562A and A121534A, collected in Tongling, Anhui, for the purpose of conducting noise removal tests. Fig. 13 depicts the pre- and postnoise removal results of the four-component time series from the TS4 files of A121562A and A121534A. The sampling rate was set at 150, and the noise removal method employed in these experiments was the one proposed in this article. Fig. 14 illustrates the variations in apparent resistivity and phase before and after noise removal for A121562A and A121534A. Analysis of Figs. 13 and 14 reveals that A121562A and A121534A were primarily affected by short-period noise, with A121534A experiencing more severe noise interference compared to A121562A. This noise resulted in distortions in their

Authorized licensed use limited to: TU Delft Library. Downloaded on February 20,2024 at 08:28:18 UTC from IEEE Xplore. Restrictions apply.

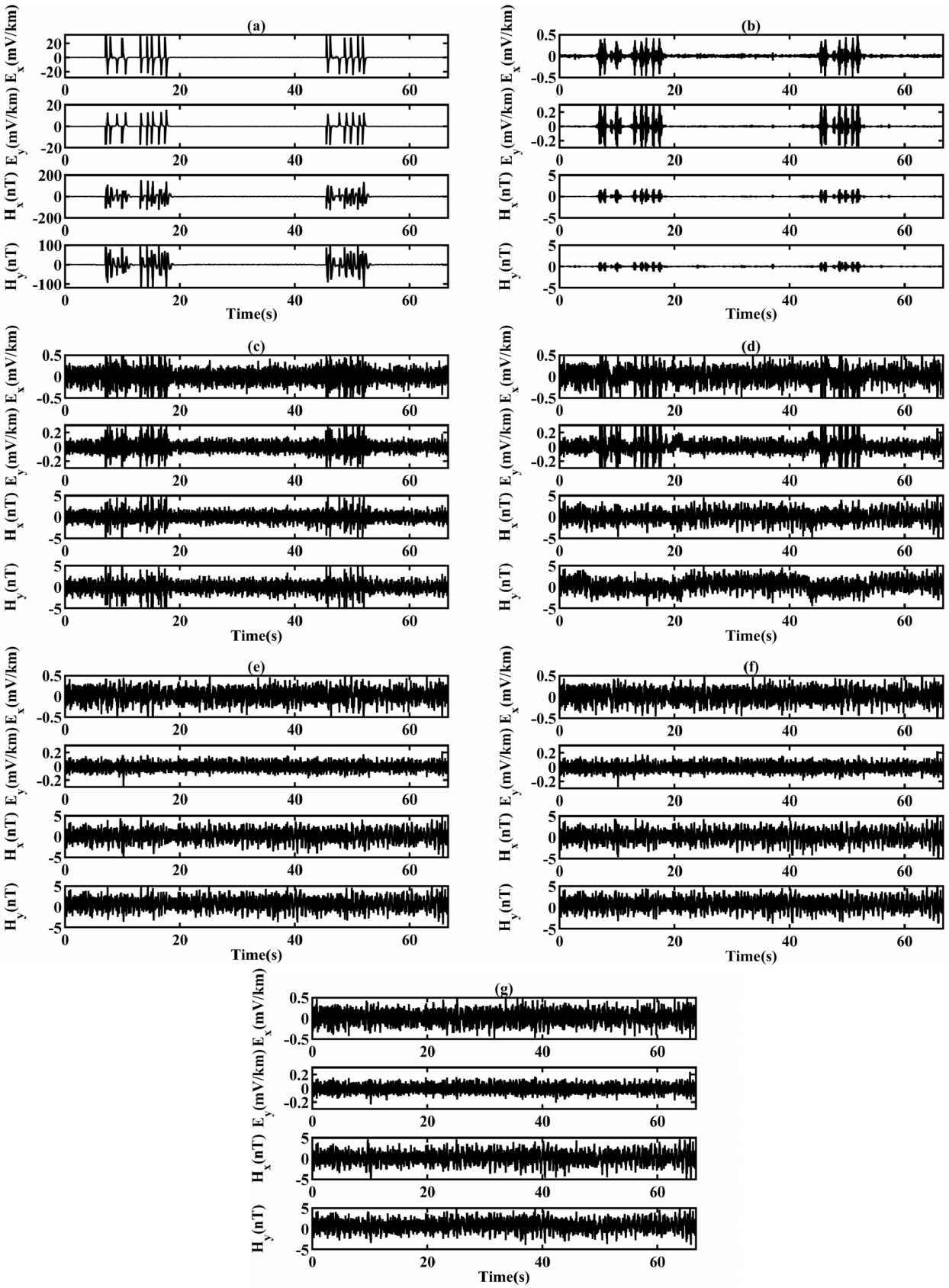

Fig. 15. Denoising results for time-series amplification sections of A121534A. (a) Noisy data. (b) VMD. (c) Wavelet transform. (d) DDTF. (e) ResNet. (f) CBAM. (g) Proposed method.

apparent resistivity and phase measurements. The proposed method effectively mitigated noise interference at these two measurement points, as evidenced by the absence of discernible noise interference in their time series after noise

Authorized licensed use limited to: TU Delft Library. Downloaded on February 20,2024 at 08:28:18 UTC from IEEE Xplore. Restrictions apply.

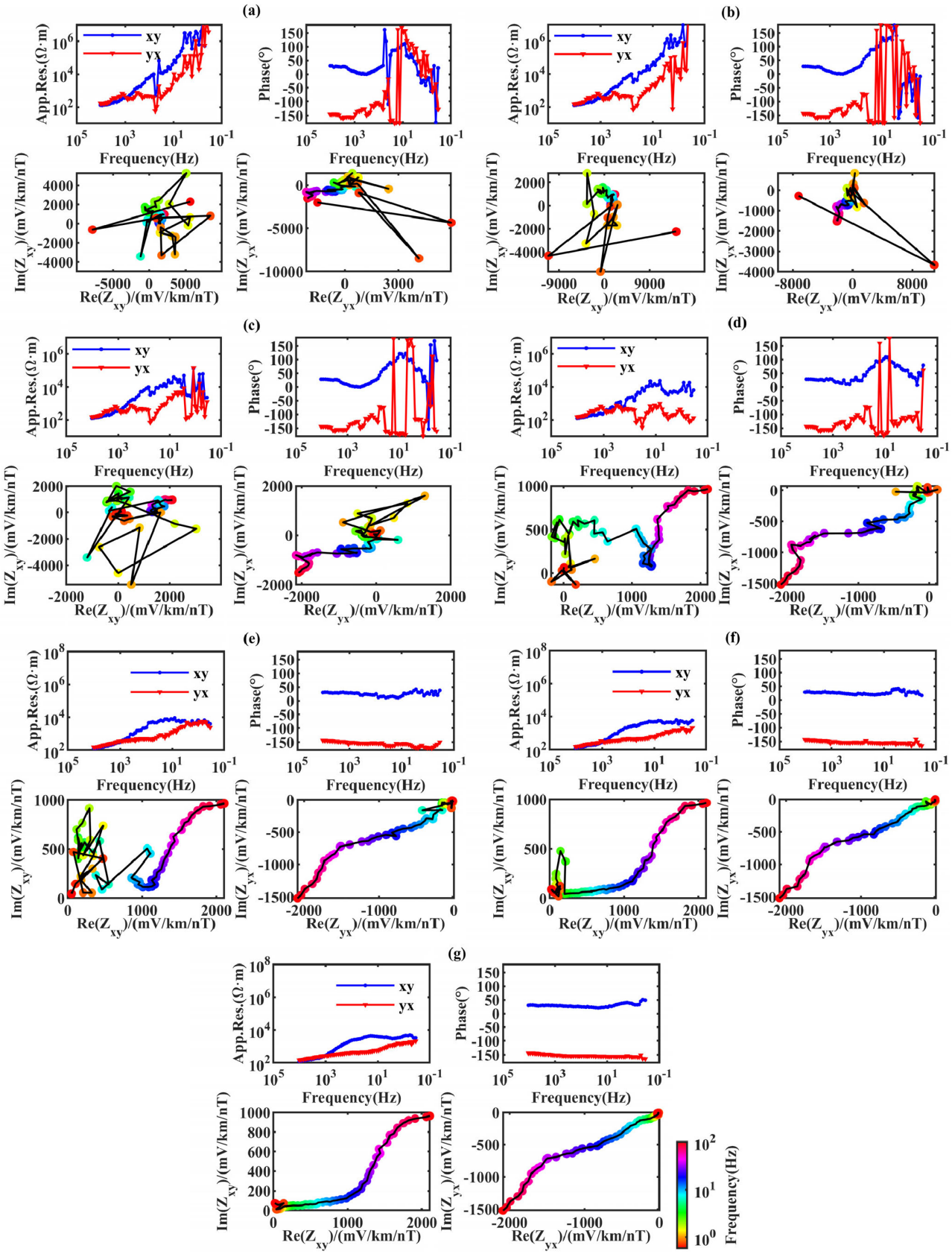

Fig. 16. Denoising results for apparent resistivity, phase, and Nyquist diagram of A121534A. (a) Noisy data. (b) VMD. (c) Wavelet transform. (d) DDTF. (e) ResNet. (f) CBAM. (g) Proposed method.

removal. Additionally, apart from a few isolated frequency points, their apparent resistivity and phase curves exhibited continuous and smooth behavior.

To effectively demonstrate the superiority of the proposed method in AMT noise removal, we present a detailed showcase using the heavily noise-affected measurement point A121534A

Authorized licensed use limited to: TU Delft Library. Downloaded on February 20,2024 at 08:28:18 UTC from IEEE Xplore. Restrictions apply.

as an example. We magnified a segment of the time series between 1680 and 1745 s from A121534A, and the resulting amplification is shown in Fig. 15(a). From Fig. 15(a), it is evident that this particular time segment is primarily disturbed by a discharge-like triangular waveform. We performed noise removal on this noisy segment using various methods, including VMD, wavelet transform, DDTF, ResNet, CBAM, and the method proposed in this study. The respective results are presented in Fig. 15(b)–(g). Analysis of Fig. 15 reveals that VMD and wavelet transform struggle to handle abrupt noise, resulting in poor noise removal outcomes with significant residual noise in the time series, thereby significantly attenuating the AMT signal. DDTF performs slightly better than VMD and wavelet transform, with a smaller amount of residual noise. However, it also compromises the noise-free signal, as evident from the noticeable rise in the time series of the magnetic component. The noise removal results obtained from ResNet, CBAM, and the proposed method outperform the previous three methods, exhibiting minimal residual noise and effectively preserving the noise-free signal. Notably, the proposed method exhibits the least amount of residual noise among the comparative methods.

Fig. 16 displays the apparent resistivity and phase curves of A121534A, demonstrating the performance of various noise suppression methods, namely, VMD, wavelet transform, DDTF, ResNet, CBAM, and the proposed method. However, it should be noted that the smoothness and continuity of the apparent resistivity and phase curves in AMT measurements do not necessarily imply the absence of noise in the time series. For a high-quality AMT measurement, in addition to being smooth and continuous, the impedance must also satisfy the special discrete relationship of the Hilbert transform. This relationship can be determined by plotting a Nyquist diagram: by mapping the real and imaginary parts of the impedance onto a 2-D plane, the impedance points projected onto the coordinate axes exhibit a clockwise trend from low to high frequencies [41], [42]. Therefore, in Fig. 16, we also present the corresponding Nyquist diagrams to assess the denoising performance of each method.

From Fig. 16, it is evident that prior to denoising, the apparent resistivity, phase, and Nyquist diagrams of A121534A exhibit severe distortion. After applying VMD and wavelet transform for denoising, the apparent resistivity and phase curves remain relatively chaotic, and the Nyquist diagrams do not exhibit a clockwise trend. The denoising results obtained from DDTF show improved morphologies of the apparent resistivity and phase curves compared to VMD and wavelet transform. The Nyquist diagram after DDTF denoising vaguely exhibits a clockwise trend, albeit with significant fluctuations in the low-frequency range. The apparent resistivity and phase curves after denoising with ResNet and CBAM become more continuous, and their Nyquist diagrams exhibit a clear clockwise trend. However, significant fluctuations still persist in the low-frequency range. The proposed method yields superior morphologies of the apparent resistivity and phase curves compared to ResNet and CBAM, with a distinct clockwise trend observed in the Nyquist diagram. Additionally, the proposed method exhibits minimal fluctuations in the low-frequency range.

V. Conclusion

In response to the issue of decreased denoising accuracy in current deep-learning-based AMT denoising methods due to the neglect of AMT signal characteristics, we propose a CBAM-based AMT multicomponent noise identification and suppression method. This method improves the process from three aspects: the establishment of the sample set, the construction of the neural network, and the design of the denoising procedure. In the establishment of the sample set, to balance noise interference and realism, an equal number of synthetic and field data are used to construct the sample set. A time window is employed to select data segments from the AMT electric and magnetic four components simultaneously, ensuring that the constructed sample set contains the correlation features of the noise, enabling the network to explore the underlying connections between the components and establish stronger mapping relationships to enhance the denoising effect. In the construction of the neural network, to enhance the network's ability to learn noise features, CBAM is incorporated into the residual block structure of ResNet, allowing the network to better focus on the feature information. In the design of the denoising procedure, based on the local concentration of short-period noise, a process of identification before denoising is adopted. After identifying the segments containing noise, noise suppression is applied only to these segments to protect the noise-free segments from being compromised during the denoising process, thereby improving denoising accuracy. The effectiveness of our proposed method is validated through experiments using both synthetic and field data. In comparative experiments, we compare our method with other time-frequency denoising methods such as VMD, wavelet transform, DDTF, ResNet, and CBAM. Through analysis of SNR, apparent resistivity and phase curves, and Nyquist diagrams, we conclude that our method achieves high-precision AMT denoising and outperforms the compared methods. Additionally, we compare the influence of different time window lengths on noise identification and suppression.

In addition to achieving accurate AMT denoising, the proposed method possesses several advantages. First, it is closely related to the geological information and noise sources of the measurement points. By utilizing high-quality data segments from the current and neighboring measurement points, along with noise samples, the constructed sample set not only includes the geological structural information of the measurement points but also incorporates the noise characteristics of nearby interference sources. Consequently, during training, the neural network learns these relevant features. Second, the proposed method exhibits robustness against noise. By incorporating synthetic data generated through geological forward modeling in the construction of the sample set, the neural network can still learn the correct mapping relationship even if the field data in the sample set are contaminated by noise. This encourages the neural network to strike a balance between constructing denoising and geological information mappings. Third, the method demonstrates excellent scalability and stability. It extends the conventional ResNet18 by incorporating the CBAM structure into the residual blocks. When there is a need to construct a larger sample set with richer noise information features, the main structure of the network can be

Authorized licensed use limited to: TU Delft Library. Downloaded on February 20,2024 at 08:28:18 UTC from IEEE Xplore. Restrictions apply.

expanded from ResNet18 to ResNet34, ResNet50, ResNet101, ResNet152, and other conventional ResNet network families, while the CBAM structure remains added to the residual blocks. This architecture allows the network to accommodate a greater amount of information from the sample set, facilitating the deepening of the network. Therefore, the proposed method holds significant industrial application value.

While the method proposed in this article partially addresses the drawback of decreased denoising accuracy in deep learning methods due to the neglect of AMT signal characteristics, it still faces the following issues. First, the sample proportions and size parameters need further testing. In constructing the sample set, this study selected synthetic data and field data in the same proportion without examining the impact of different sample proportions on AMT denoising effectiveness. Additionally, regarding the selection of sample size, only the performance impact of sample lengths of 128, 256, 512, and 1024 was tested. Second, the network structure and training method require optimization. Compared to conventional deep learning AMT denoising methods, this study employs a sample set with increased dimensions and a more complex neural network structure, resulting in longer training times and increased difficulty in parameter tuning. Therefore, further adjustments to the network structure and the adoption of faster network training methods are necessary. Third, the network performance deteriorates when dealing with long-period noise. The process of identification preceding denoising becomes cumbersome when handling long-period noise, rendering the identification process meaningless. Moreover, when long-period noise pervades the entire AMT time series, it becomes challenging to select high-quality data segments for constructing the sample set. Consequently, the denoising mapping constructed by the network becomes more reliant on the synthetic data in the sample set, exacerbating the problem of deviating from real-world scenarios. In summary, further testing of the influence of sample proportions and size parameters on the neural network, optimization of the network structure, and exploration of faster optimization algorithms, as well as the introduction of mechanisms for identifying and denoising long-period noise, represent potential future directions for deep learning in AMT denoising research.

ACKNOWLEDGMENT

Special thanks are given to Shuanggui Hu, Cong Zhou, and anonymous reviewers for their careful work and thoughtful suggestions that have helped improve this article substantially.

REFERENCES

[1] A. Ádám et al., "Magnetotelluric and audiomagnetotelluric measurements in Finland," *Tectonophysics*, vol. 90, nos. 1–2, pp. 77–90, Dec. 1982.

[2] A. D. Chave and A. G. Jones, *The Magnetotelluric Method: Theory and Practice*. Cambridge, U.K.: Cambridge Univ. Press, 2012.

[3] G. Li et al., "Near-source noise suppression of AMT by compressive sensing and mathematical morphology filtering," *Appl. Geophys.*, vol. 14, no. 4, pp. 581–589, Dec. 2017.

[4] T. D. Gamble, W. M. Goubau, and J. Clarke, "Magnetotellurics with a remote magnetic reference," *Geophysics*, vol. 44, no. 1, pp. 53–68, Jan. 1979.

[5] Z. Guo et al., "Research on a multiscale denoising method for low signal-to-noise magnetotelluric signal," *IEEE Trans. Geosci. Remote Sens.*, vol. 60, 2022, Art. no. 5925018.

[6] D. Sutarno and K. Vozoff, "Robust M-estimation of magnetotelluric impedance tensors," *Exploration Geophys.*, vol. 20, no. 3, pp. 383–398, Jun. 1989.

[7] A. D. Chave and D. J. Thomson, "A bounded influence regression estimator based on the statistics of the hat matrix," *J. Roy. Stat. Soc. Ser. C, Appl. Statist.*, vol. 52, no. 3, pp. 307–322, Jul. 2003.

[8] M. Y. Smirnov, "Magnetotelluric data processing with a robust statistical procedure having a high breakdown point," *Geophys. J. Int.*, vol. 152, no. 1, pp. 1–7, Jan. 2003.

[9] G. D. Egbert and D. W. Livelybrooks, "Single station magnetotelluric impedance estimation: Coherence weighting and the regression M-estimate," *Geophysics*, vol. 61, no. 4, pp. 964–970, Jul. 1996.

[10] R. L. Parker, "The inverse problem of electromagnetic induction: Existence and construction of solutions based on incomplete data," *J. Geophys. Res., Solid Earth*, vol. 85, no. B8, pp. 4421–4428, Aug. 1980.

[11] C. Zhou et al., "Application of the Rhoplus method to audio magnetotelluric dead band distortion data," *Chin. J. Geophys.*, vol. 58, no. 12, pp. 4648–4660, 2015.

[12] G. Li, X. Liu, J. Tang, J. Li, Z. Ren, and C. Chen, "De-noising low-frequency magnetotelluric data using mathematical morphology filtering and sparse representation," *J. Appl. Geophys.*, vol. 172, Jan. 2020, Art. no. 103919.

[13] C. Jian-Hua, "A combinatorial filtering method for magnetotelluric data series with strong interference," *Arabian J. Geosci.*, vol. 9, no. 13, pp. 1–10, Sep. 2016.

[14] J. Li, F. Ma, J. Tang, Y. Liu, and J. Cai, "Denoising application of magnetotelluric low-frequency signal processing," *IEEE Trans. Geosci. Remote Sens.*, vol. 60, 2022, Art. no. 5920518.

[15] J. Li, X. Zhang, and J. Tang, "Noise suppression for magnetotelluric using variational mode decomposition and detrended fluctuation analysis," *J. Appl. Geophys.*, vol. 180, Sep. 2020, Art. no. 104127.

[16] Z. Wang, Y. Liu, J. Du, Z. Wang, and Q. Shao, "De-noising magnetotelluric data using variational mode decomposition combined with mathematical morphology filtering and wavelet thresholding," *J. Appl. Geophys.*, vol. 204, Sep. 2022, Art. no. 104751.

[17] X. Zhang, D. Li, J. Li, and Y. Li, "Grey wolf optimization-based variational mode decomposition for magnetotelluric data combined with detrended fluctuation analysis," *Acta Geophysica*, vol. 70, no. 1, pp. 111–120, Feb. 2022.

[18] Z. Ling, P. Wang, Y. Wan, and T. Li, "Effective denoising of magnetotelluric (MT) data using a combined wavelet method," *Acta Geophysica*, vol. 67, no. 3, pp. 813–824, Jun. 2019.

[19] D. O. Trad and J. M. Travassos, "Wavelet filtering of magnetotelluric data," *Geophysics*, vol. 65, no. 2, pp. 482–491, Mar. 2000.

[20] J. Li, Y. Peng, J. Tang, and Y. Li, "Denoising of magnetotelluric data using K-SVD dictionary training," *Geophys. Prospecting*, vol. 69, no. 2, pp. 448–473, Feb. 2021.

[21] G. Li et al., "Improved shift-invariant sparse coding for noise attenuation of magnetotelluric data," *Earth, Planets Space*, vol. 72, no. 1, pp. 1–15, Dec. 2020.

[22] L. Zhang, J. Tang, G. Li, and W. Chen, "Audio magnetotelluric denoising via variational mode decomposition and adaptive dictionary learning," *J. Appl. Geophys.*, vol. 204, Sep. 2022, Art. no. 104748.

[23] L. Zhang et al., "Seismic data denoising using double sparsity dictionary and alternating direction method of multipliers," *J. Seismic Explor.*, vol. 29, no. 1, pp. 49–71, 2020.

[24] G. Li et al., "IncepTCN: A new deep temporal convolutional network combined with dictionary learning for strong cultural noise elimination of controlled-source electromagnetic data," *Geophysics*, vol. 88, no. 4, pp. E107–E122, Jul. 2023.

[25] J. Li, Y. Liu, J. Tang, Y. Peng, X. Zhang, and Y. Li, "Magnetotelluric data denoising method combining two deep-learning-based models," *Geophysics*, vol. 88, no. 1, pp. E13–E28, Jan. 2023.

[26] J. Li, Y. Liu, J. Tang, and F. Ma, "Magnetotelluric noise suppression via convolutional neural network," *Geophysics*, vol. 88, no. 1, pp. WA361–WA375, Jan. 2023.

[27] L. Zhang, Z. Ren, X. Xiao, J. Tang, and G. Li, "Identification and suppression of magnetotelluric noise via a deep residual network," *Minerals*, vol. 12, no. 6, p. 766, Jun. 2022.

[28] G. Li et al., "Multitype geomagnetic noise removal via an improved U-Net deep learning network," *IEEE Trans. Geosci. Remote Sens.*, vol. 61, 2023, Art. no. 5916512.

[29] D. P. Kingma and J. Ba, "Adam: A method for stochastic optimization," 2014, *arXiv:1412.6980*.

Authorized licensed use limited to: TU Delft Library. Downloaded on February 20,2024 at 08:28:18 UTC from IEEE Xplore. Restrictions apply.

[30] J. Sun, S. Slang, T. Elboth, T. Larsen Greiner, S. McDonald, and L.-J. Gelius, "A convolutional neural network approach to deblending seismic data," *Geophysics*, vol. 85, no. 4, pp. WA13–WA26, Jul. 2020.
[31] P. Wang, X. Chen, and Y. Zhang, "Synthesizing magnetotelluric time series based on forward modeling," *Frontiers Earth Sci.*, vol. 11, Feb. 2023, Art. no. 1086749.
[32] Z. Liu et al., "Deep learning audio magnetotellurics inversion using residual-based deep convolution neural network," *J. Appl. Geophys.*, vol. 188, May 2021, Art. no. 104309.
[33] H. Li, W. Yang, X. Zhang, X. Wei, and X. Xu, "A ResNet-based method for complex channel interpretation in seismic volumes," *IEEE Geosci. Remote Sens. Lett.*, vol. 19, pp. 1–5, 2022.
[34] S. Zhang and N. Zhou, "Extraction of multiple electrical parameters from IP-affected transient electromagnetic data based on LSTM-ResNet," *IEEE Trans. Geosci. Remote Sens.*, vol. 61, 2023, Art. no. 4501614.
[35] C. Szegedy et al., "Inception-v4, inception-ResNet and the impact of residual connections on learning," in *Proc. AAAI Conf. Artif. Intell.*, 2017, vol. 31, no. 1, pp. 4278–4284.
[36] V. C. Dodda, L. Kuruguntla, A. K. Mandpura, and K. Elumalai, "Simultaneous seismic data denoising and reconstruction with attention-based wavelet-convolutional neural network," *IEEE Trans. Geosci. Remote Sens.*, vol. 61, 2023, Art. no. 5908814.
[37] J. Wang et al., "Automated ECG classification using a non-local convolutional block attention module," *Comput. Methods Programs Biomed.*, vol. 203, May 2021, Art. no. 106006.
[38] S. Woo et al., "Cbam: Convolutional block attention module," in *Proc. Eur. Conf. Comput. Vis. (ECCV)*, 2018, pp. 3–19.
[39] Y. Lou et al., "Irregularly sampled seismic data interpolation via wavelet-based convolutional block attention deep learning," *Artif. Intell. Geosci.*, vol. 3, pp. 192–202, Dec. 2022.
[40] J. Li et al., "Application of GPR system with convolutional neural network algorithm based on attention mechanism to oil pipeline leakage detection," *Frontiers Earth Sci.*, vol. 10, May 2022, Art. no. 863730.
[41] J. Uhm, J. Heo, D.-J. Min, S. Oh, and H.-J. Chung, "Imaging strategies to interpret 3-D noisy audio-magnetotelluric data acquired in Gyeongju, South Korea: Data processing and inversion," *Geophys. J. Int.*, vol. 225, no. 1, pp. 744–758, Dec. 2020.
[42] Y. Yue et al., "Magnetotelluric transfer function distortion assessment using Nyquist diagrams," *J. Appl. Geophys.*, vol. 160, pp. 218–228, Jan. 2019.

Liang Zhang (Member, IEEE) received the B.S. and M.S. degrees from Jilin University, Changchun, China, in 2015 and 2018, respectively, and the Ph.D. degree from Central South University, Changsha, China, in 2022.

He is currently a Lecturer with Guizhou University, Guiyang, China. His research interests include machine learning and magnetotelluric signal denoising.

Guang Li received the B.S. and M.S. degrees from the Hunan University of Science and Technology, Xiangtan, China, in 2011 and 2014, respectively, and the Ph.D. degree from Central South University, Changsha, China, in 2018.

He is currently an Associate Professor with the East China University of Technology, Nanchang, China. His research interests are geophysical data processing and its applications to probe the Earth's interior.

Huang Chen received the B.S. and Ph.D. degrees from Central South University, Changsha, China, in 2015 and 2022, respectively.

He is currently an Assistant Researcher with Chongqing University, Chongqing, China. His research mainly focuses on geo-electric and geo-electromagnetic forward and inverse modeling, and the corresponding data processing.

Jingtian Tang received the B.S. and M.S. degrees from Jilin University, Changchun, China, in 1985 and 1988, respectively, and the Ph.D. degree from Central South University, Changsha, China, in 1992.

In 1998, he visited the Lawrence Berkeley National Laboratory, Berkeley, CA, USA, as a Senior Visiting Scholar. He is currently a Professor with Central South University. His research interests include the theory, instruments, and applications of electromagnetic sounding.

Guanci Yang received the B.S. degree from the Hunan Institute of Science and Technology, Yueyang, China, in 2006, the M.S. degree from Guizhou University, Guiyang, China, in 2009, and the Ph.D. degree from the University of Chinese Academy of Sciences, Chengdu, China, in 2012.

In 2015, he visited Oklahoma State University, Stillwater, OK, USA, as a Visiting Scholar. He is currently a Professor with Guizhou University. His research interests include deep learning and optimization algorithm.

Mingbiao Yu (Member, IEEE) received the B.E. degree from the University of South China, Hengyang, China, in 2010, the M.S. degree from Jiangsu University, Zhenjiang, China, in 2013, and the Ph.D. degree from Southeast University, Wuhan, China, in 2019.

He is currently a Lecturer with Guizhou University, Guiyang, China. His research interests mainly focus on geophysical instruments research.

Yong Hu received the B.S. and Ph.D. degrees from Jilin University, Changchun, China, in 2014 and 2019, respectively.

From 2017 to 2018, he was a Joint Ph.D. Student with the University of California, Santa Cruz, CA, USA. He is currently an Associate Professor with the China University of Mining and Technology, Xuzhou, China. His research interests include geophysical data processing and seismic full-waveform inversion and imaging.

Jun Xu received the B.S. degree from Guizhou University, Guiyang, China, in 2015, where he is currently pursuing the M.S. degree.

His research interests include machine learning and signal denoising.

Jing Sun received the B.S. and M.S. degrees from Jilin University, Changchun, China, in 2015 and 2018, respectively, and the Ph.D. degree from the University of Oslo, Oslo, Norway, in 2022.

She is currently an Assistant Professor with the Intelligent Systems Department, Delft University of Technology, Delft, The Netherlands. Her research interests include machine learning for resolving geophysical challenges.

Authorized licensed use limited to: TU Delft Library. Downloaded on February 20,2024 at 08:28:18 UTC from IEEE Xplore. Restrictions apply.